

Research article

Graphitic C₃N₄ incorporated chitosan-poly(vinyl alcohol) blend nanocomposites for the removal of Cu(II) and Cr(VI) ions from aqueous solutions

Shivapura Manchaiah Anush¹, Suchetha Naga Raju², Ballupet Honnappa Gayathri³,
Keresanthe Parameshwarappa Ajeya¹, Yarabahally Ravindranath Girish¹,
Sanneerappa Darshan¹, Yelaware Puttaswamy Naveen¹, Kalappa Prashantha^{1*},
Byrappa Krishnaiah Narendra⁴, Aishwarya Jayaram⁵

¹Centre for Research and Innovation, Adichunchanagiri School of Natural Sciences, Adichunchanagiri University, 571448 Mandya, India

²Department of Polymer Science and Technology, JSS Science and Technology University, 570006 Mysore, India

³BMS College for Women, Basavanagudi, Bengaluru, 560004 Karnataka, India

⁴BGS Institute of Technology, Adichunchanagiri University, 571448 Mandya, India

⁵Vidyavardhaka College of Engineering, 570002 Mysore, India

Received 7 August 2023; accepted in revised form 24 October 2023

Abstract. A novel adsorbent material for the effective removal of hazardous metal ions from aqueous solutions was developed through modifications to chitosan. The process involved the use of vanillin to create cross-linked chitosan, which was then combined with thiourea-based graphitic carbon nitride (g-C₃N₄) to form a gel matrix. The resulting composite material was thoroughly characterized using various techniques, including Fourier transform infrared spectroscopy, thermogravimetric analysis, scanning electron microscopy, energy dispersive X-ray spectroscopy, and X-ray diffractometry. To assess its efficacy, adsorption experiments were conducted to determine the capability of the synthesized compounds to adsorb Cu(II) and Cr(VI) ions. The observed results found that the adsorption process was found to follow pseudo-second-order kinetics and the Langmuir isotherm model. Through thermodynamic studies, it was revealed that the adsorption process was both endothermic and spontaneous in nature. Furthermore, desorption studies confirmed that the material could be regenerated, making it reusable. This characteristic allowed for the effective recovery of the adsorbate species and highlighted the potential for reusing the adsorbent material multiple times.

Keywords: chitosan, polyvinyl alcohol, graphitic C₃N₄, metal ion removal

1. Introduction

The rapidly increasing human population and their needs have led to increased industrialization. Effluents from the industries led to increased environmental pollution, creating serious environmental issues. Effluents contain numerous heavy metal ions, which are highly toxic and debilitating to humans as well as other living organisms. Effluents from the industries become an on-pressing issue as the toxic metal

ions and the dye contents get mixed and further cause major environmental issues [1–3]. These heavy metals are of severe risk since they can show toxicity at minute concentrations and are mainly not degraded by natural processes [4, 5].

Copper is one of the toxic metal ions that have been used by various industries for the production of materials such as paper, leather, petroleum refining, etc. Chromium ion pollution is a result of events of nature,

*Corresponding author, e-mail: prashantha.kalappa@gmail.com

© BME-PT

including volcanic eruption and the attrition of mercury-loaded sediments and synthetic industries such as metal plating and dyeing industries. Cr in the (III) oxidation state is less toxic compared to Cr in the (VI) state. The less toxic Cr(III) can be easily removed from wastewater as $\text{Cr}(\text{OH})_3$ in the precipitated form; however, the reduction of Cr(VI) to Cr(III) is a difficult task in the adsorptive process during water purification [6]. The presence of these metal ions in the drinking water is highly harmful and causes serious illnesses such as damaging the nervous system and reproductive system, mucosal irritation, hepatic and renal damage, and in some cases, nerve problems followed by depression and gastrointestinal irritation [7]. The maximum acceptable concentration of these metals, such as Cr(VI) and Cu(II), in potable water is 2.0 and 0.02 mg/l, respectively. The management of these effluents is one of the basic necessities for human health; therefore, much attention has been given by researchers to the removal of these toxic ions from the effluents by employing various methods such as adsorption [8]. Precipitation [9], ion exchange [10], reverse osmosis [11], and membrane separation [12]. Among these methods, adsorption is one of the most commonly used, easy, and reliable methods and has a high-efficiency rate; its high selectivity and cost-effectiveness have made it a promising material for the treatment of wastewater [13–15].

Several adsorbent materials have been widely investigated for the adsorption of toxic ions and their removal from wastewater. The materials such as activated clay, carbon materials, carbon nanotubes, polymeric materials, and activated carbon [16–20]. The introduction of smart adsorbent materials provides a large surface area and porosity, reduces adsorption time, and increases the adsorption efficiency [21]. However, the synthesis of some adsorbent materials needs some complicated procedures and is quite expensive, so the researchers are focusing on developing adsorbent materials that are easy to synthesize and would be economically favorable; thus, our task in this research work is to develop a novel material for wastewater treatment. Along with the above properties, the adsorbent material should be biodegradable after its stipulated number of uses [22–24]. Hence, polysaccharide-based adsorbent materials are being investigated as adsorbent materials in the treatment of adsorbent-based wastewater treatment.

Chitosan (CS), a polycationic unbranched polysaccharide derived from chitin, is one of the promising natural adsorbent materials because of its unique properties viz., such as biocompatibility, biodegradability, cytocompatibility, and hemocompatibility [25, 26]. Due to its macromolecular structure and its reactive functional groups, it results in increased adsorption and binding capacity. Its metal chelating property and cationicity in acidic solution, so it has been made selective for the adsorption process. Also, it acts as a good dispersant, so the interaction between the metal and the gel matrix takes place evenly so that excellent adsorptive properties can be obtained. Several researchers have focused on the modification of chitosan by introducing new functional groups that help enhance the adsorptive property [26]. Also, the addition of polyvinyl alcohol (PVA) to the chitosan strengthens the matrix by immobilizing within it, forming H-bonds with the amino groups of chitosan and providing more active sites for the adsorption process.

Carbon nitride (C_3N_4) is one of the most promising materials possessing excellent properties such as hardness, good mechanical properties, low friction coefficient, and useful optical and electronic properties. Five different structures of carbon nitride are available as per the theoretical calculations. Among the 5 structures, more attention has been shown towards (graphitic carbon nitride) g- C_3N_4 material due to its stability when compared to the other 4 structures. g- C_3N_4 is a π -conjugated material and has been used extensively in many fields, such as bioimaging, metal ion detectors, fuel cells, photocatalysis, photo conduction; hydrogen evaluation and CO_2 capture. Several adsorbent materials have been reported using g- C_3N_4 for the adsorptive removal of toxic metal ions from aqueous solutions [27].

The primary objective of this study is to develop an efficient, cost-effective, environmentally friendly, and biodegradable adsorbent nanocomposite by combining g- C_3N_4 nanoparticles with chitosan-PVA as the adsorbing material. The focus is on investigating the unique hybrid nanocomposites capacity to adsorb Cu(II) and Cr(VI) ions. The research also involves analyzing the adsorption isotherms to determine the maximum adsorption capacities of these metal ions. Additionally, the study aims to assess the thermodynamic properties of the adsorption process, including changes in standard Gibbs free energy (G°), enthalpy (H°), and entropy (S°). The kinetic

adsorption parameters will be evaluated by validating them using pseudo-first-order and second-order kinetic models. Furthermore, the study will examine the reusability of the adsorbent material by evaluating its regeneration process, which is crucial for determining the potential for repeated usage. By achieving these objectives, the present study aims to contribute to the development of an effective and sustainable solution for removing hazardous metal ions from aqueous solutions.

2. Experimental

2.1. Materials

Chitosan (CS) and polyvinyl alcohol (PVA) were purchased from M/s Sigma Aldrich (Bangalore, India). Acetic acid, potassium dichromate, copper sulphate, and thiourea were purchased from M/s Spectrochem Private Limited (Bangalore, India).

2.1.1. Synthesis of g-C₃N₄

About 10 g of thiourea was weighed and transferred to a cup-shaped crucible, which was placed in a muffle furnace and heated to 550 °C for 4 h with a heating rate of 15 °C/min to obtain the yellowish g-C₃N₄ powder [28].

2.1.2. Preparation of 2-dimensional g-C₃N₄

5 g of the prepared g-C₃N₄ material was first crushed into a fine powder. This powder was then placed in a crucible with a cover and heated for 4 hours. The heating process was carried out at a rate of 15 °C per minute, and the temperature was set to 550 °C. After the heating process, a yellowish fine powder of 2-dimensional g-C₃N₄ was obtained [28].

2.1.3. Preparation of CS/PVA/g-C₃N₄ composite (CPG)

A mass of 0.5 g of chitosan was dissolved in 40 ml of 0.5% aqueous acetic acid solution. To this solution, 0.3 g of polyvinyl alcohol previously dissolved in water was transferred and stirred for 24 h. Then 0.16 mg of g-C₃N₄ was added and sonicated for 4 h to obtain the final CPG product. The obtained CS/PVA/g-C₃N₄ product was dried in an oven to obtain the final material.

2.2. Analytical techniques

The prepared individual materials, CPG, CS and g-C₃N₄, were characterized by various analytical characterization techniques.

Fourier transform infrared spectroscopy (FTIR) (Shimadzu, Kyoto, Japan) was used in the range of 500–4000 cm⁻¹ using the IR-prestige instrument to study the possible stretching and bending vibrations of the materials.

The thermal properties of the materials were characterized by thermogravimetric analysis (TGA) using a DTG-60 (Shimadzu, Kyoto, Japan) under a N₂ atmosphere with a heating rate of 10 °C/min.

To study the crystal structure and geometry of the material, X-ray diffraction (XRD) was studied in a powder XRD instrument (Rigaku Mini Flex 600 (Tokyo, Japan) with 2θ from 0 to 90° with Cu K_α radiation).

Carl Zeiss scanning electron microscope (SEM) (AG, Jena, Germany) with an operating voltage of 5 kV was used to study the surface morphology.

2.3. Metal adsorption studies

2.3.1. Adsorption studies

Duplicate samples were utilized in batch studies to assess the adsorption capabilities of the CPG concerning the metal ions Cu(II) and Cr(VI) at various concentrations ranging from 20 to 100 mg/l. To perform the batch tests, 25 mg of the produced CPG material was mixed with known concentrations of metal ions solution and subjected to slow stirring. The remaining metal ions in the solution after the CPG application were measured at specific intervals using an atomic absorption spectrophotometer (AAS). Equation (1) was then applied to determine the equilibrium adsorption capacity (q_e) of the metal ions [mg/g]:

$$q_e = (C_0 - C_e) \cdot \frac{V}{w} \quad (1)$$

where C_0 is the initial concentration of the metal ions in the solution [mg/l], C_e is the equilibrium concentration of the metal ions in the solution [mg/l], w is the weight of the solid adsorbent [mg], and V is the volume of the aqueous solution used in the adsorption process [ml].

2.3.2. Desorption studies

The desorption studies were conducted to determine the quantity of metal ions adsorbed on the CPG material. After the metal ions were adsorbed, the CPG material was removed, washed with water, and then completely dried in an oven. Once dried, the CPG was subjected to stripping solutions containing HCl

(25 ml of pH 1.2) and NaOH (25 ml of 0.5 M) for 3 h at room temperature. The CPG had previously adsorbed metal ions during the adsorption process. The goal was to desorb the Cu(II) and Cr(VI) ions from the adsorbent.

To measure the amount of desorbed Cu(II) and Cr(VI) ions, the supernatant was analyzed using atomic absorption spectrophotometry. The percentage of desorption was calculated using the Equation (2):

$$\text{Desorption [\%]} = \frac{\text{amount of metal ion desorbed}}{\text{amount of metal ion adsorbed}} \cdot 100 \quad (2)$$

3. Results and discussion

3.1. Synthesis of CPG

Incorporation of PVA and chitosan creates PVA-CS matrix. Then, the addition of $g\text{-C}_3\text{N}_4$ to the matrix creates nanocomposite adsorbent material.

3.2. FTIR spectral characterization

FTIR spectrum of $g\text{-C}_3\text{N}_4$ (Figure 1) shows the presence of C=N, C–N, triazine, and –OH groups. Their stretching vibration frequencies are at 1640, 1410, 780, and 3337 cm^{-1} , respectively, which indicates the formation of $g\text{-C}_3\text{N}_4$.

The FTIR spectra in Figure 2 of CS clearly show the presence of the –OH stretching vibration frequency, showing a broad peak at 3286 cm^{-1} in the CS structure. Aliphatic stretching of C–H was observed at 2845 cm^{-1} , respectively. The band at 1638 cm^{-1} corresponds to the stretching vibration frequency of –NH, due to the presence of free amino groups in the chitosan. In the case of CPG, the spectrum revealed that there was a shift in the values of the –NH to 1649 cm^{-1} . Additional peaks of $g\text{-C}_3\text{N}_4$ were observed in the range 1640, 1410, and 750 cm^{-1} of

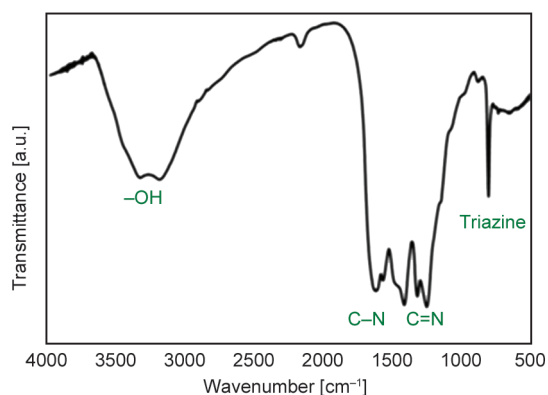


Figure 1. FTIR spectrum of $g\text{-C}_3\text{N}_4$.

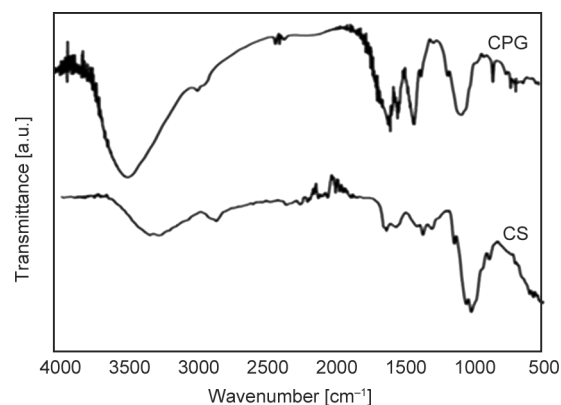


Figure 2. FTIR spectra of CS and CPG.

C=N, C–N, and triazine, and also a broad peak was observed at 3400 cm^{-1} due to the –OH stretching vibrations. The shift of the peaks is possibly due to the intra/inter molecular hydrogen bonding formed by the interaction of CS/PVA and $g\text{-C}_3\text{N}_4$.

3.3. Thermogravimetric analysis

CS showed a three-step degradation process in the temperature range of 30–600 $^{\circ}\text{C}$ (Figure 3). First step degradation was due to a weight loss of around 13% which took place in the heating range from 30 to 150 $^{\circ}\text{C}$; it is due to the evaporation of absorbed moisture of the CS matrix. In the second step of degradation, a major weight reduction took place due to the decomposition of polysaccharide chains within the structure in the heating range of 225 to 340 $^{\circ}\text{C}$, and the final degradation takes place in the range of 340–600 $^{\circ}\text{C}$ with a weight loss of 33% which shows the complete degradation or the loss of the material. The b curve shows the thermal degradation of CPG in the temperature zone of 30–600 $^{\circ}\text{C}$. The first step degradation was also due to the loss of absorbed moisture content which took place with a weight loss of 10% in the temperature zone of 30–150 $^{\circ}\text{C}$. In the second

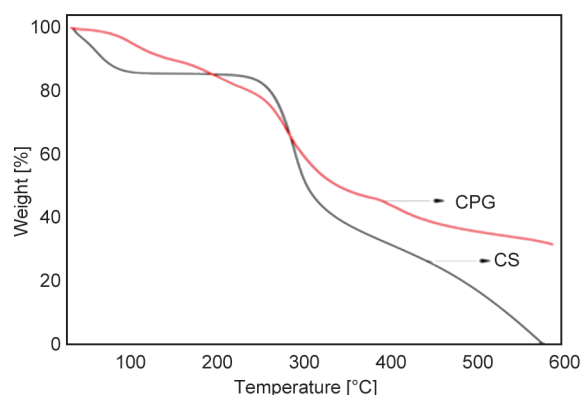


Figure 3. Thermograms of CS and CPG.

step, a weight loss of 40% was observed in the temperature zone of 220–360 °C due to the decomposition of the polymer matrix of chitosan and PVA. The final step of degradation was due to the decomposition of the g-C₃N₄ moiety, where a mass of 30% was left behind as residual matter in the temperature range of 380–600 °C.

3.4. X-ray diffraction

The X-ray diffractogram patterns of CS, g-C₃N₄, and CPG are shown in Figure 4. The peaks displayed at $2\theta = 11^\circ$ and 29° of g-C₃N₄ indicate the semi-crystalline nature. In CS, peaks appeared at $2\theta = 9^\circ$ and 21° , which also indicates the semi-crystalline nature of the sample. In CPG, a prominent wide band is seen at $2\theta = 23^\circ$ and small peaks at 8° , 14° , and 29° , which represents the semi-crystalline nature of the sample. These new peaks indicate the presence of the g-C₃N₄ in the CPG, and the surface morphology changed due to the blending of the CS, PVA, and g-C₃N₄.

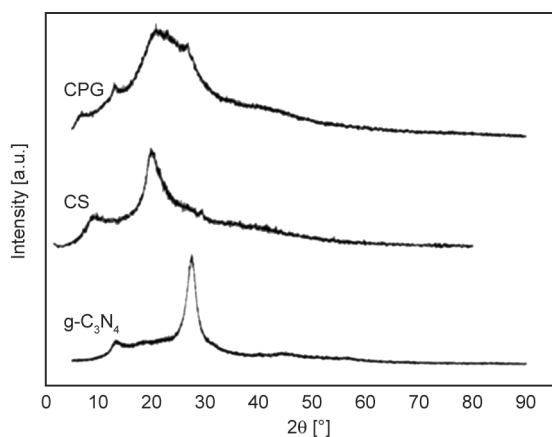


Figure 4. XRD pattern of g-C₃N₄, CS and CPG.

3.5. Scanning electron microscopy

The scanning electron microscopy (SEM) images show the morphologies of CS/PVA/g-C₃N₄ (CPG) nanocomposites, Cu(II) adsorbed on CPG, and Cr(VI) adsorbed on CPG (Figure 5). The CPG micrographs (Figure 5a) displayed a regular structure with a smooth surface and tiny rocky morphology

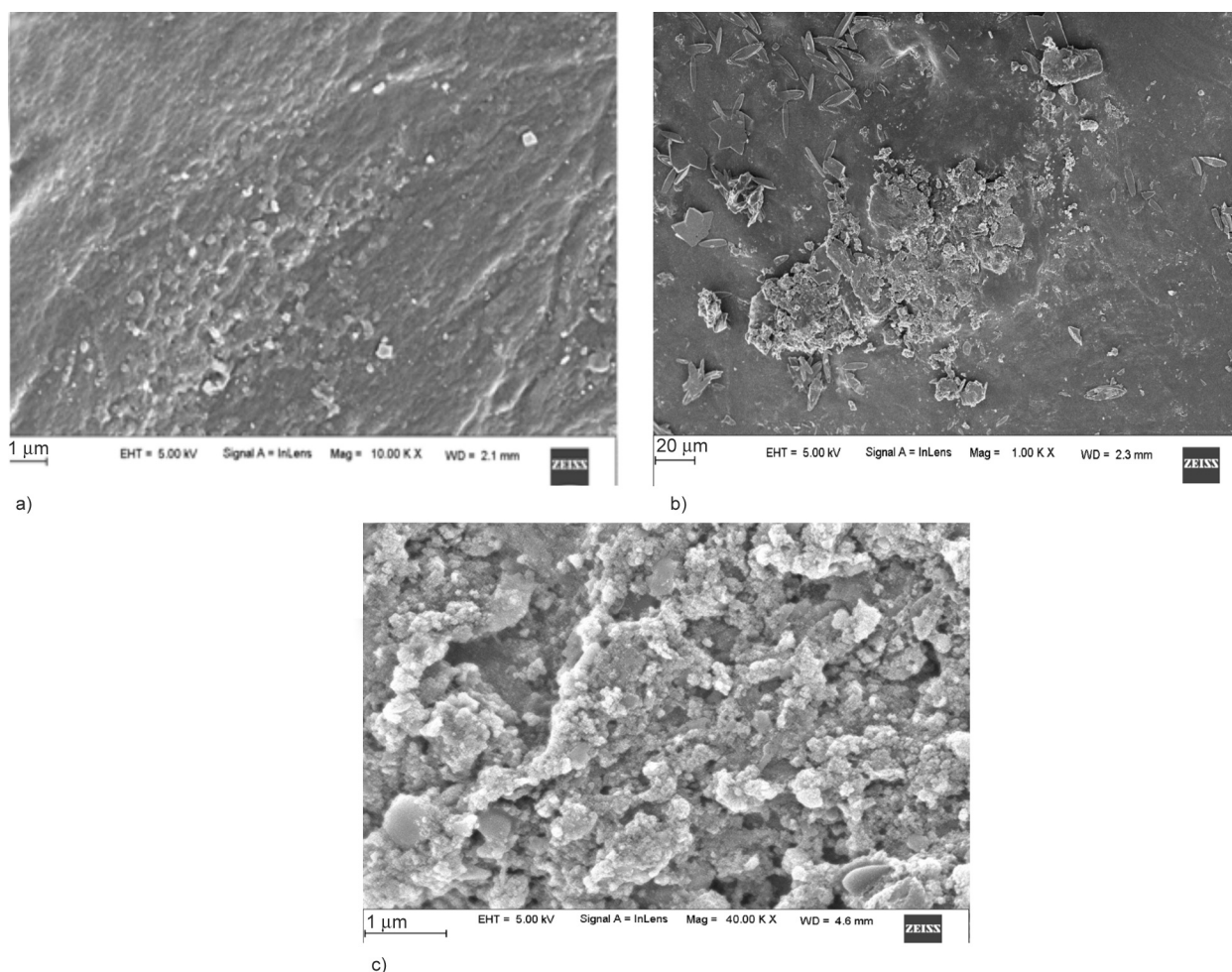


Figure 5. SEM images of a) CPG, b) Cu(II) adsorbed on CPG and, c) Cr(VI) adsorbed on CPG.

because of the addition of $g\text{-C}_3\text{N}_4$, the morphology of the sample changed drastically, as it formed nanocomposites indicating the dispersion of the nanoparticles in the polymer matrix. The micrograph of Cu(II) adsorbed on CPG (Figure 5b) and Cr(VI) adsorbed on CPG (Figure 5c), which indicates the deposition of Cu(II) and Cr(VI) ions on the CPG.

3.6. Adsorption

Figure 6 illustrates the energy dispersive X-ray spectrum (EDS) of the adsorbed Cu(II) and Cr(VI) ions. In Figure 6a, a peak is observed at 8 keV, indicating the presence of Cu(II). Additionally, peaks corresponding to carbon, nitrogen, and oxygen are evident at 0.2, 0.4, and 0.6 keV, respectively. For the adsorbed chromium sample (Figure 6b), peaks are observed at energies of 0.5, 5.5, and 5.9 keV, signifying the presence of Cr(VI). Furthermore, carbon, nitrogen, and oxygen peaks are observed at energies of 0.2 and 0.6 keV.

The interaction between metal ions and the composite material is mainly governed by the presence of functional groups. Hetero atoms, such as nitrogen, oxygen, and sulfur, play a crucial role in enhancing the adsorption process due to their electron-rich nature. The current synthetic materials contain numerous nitrogen and oxygen atoms, which contribute to the increased electrostatic adsorption of metal ions [29]. Additionally, the incorporation of $g\text{-C}_3\text{N}_4$ in the composite material results in providing a larger surface area, further enhancing the adsorption capacity. The adsorption of Cu(II) at neutral pH is attributed to two main factors. Firstly, a coordinate bond forms between the nitrogen atoms in the composite material and the metal cations. Secondly, an electrostatic interaction occurs between the nitrogen atoms and the

metal cations based on their respective charges. Both of these mechanisms contribute to the successful adsorption of Cu(II) under neutral pH conditions.

However, the adsorption capacity decreases below pH 7 due to the protonation of amines present in the composite material. This protonation process affects the availability and accessibility of active sites, leading to a reduction in Cu(II) adsorption efficiency.

For the adsorption of chromium in the hexavalent state, experiments were conducted at pH 3, as indicated by the stability diagram of the Cr(VI)-H₂O system [30]. It is important to note that at pH values below 4, the most active and noticeable species is HCrO_4^- , while $\text{Cr}_2\text{O}_7^{2-}$ predominates at pH ranges above 7.5. When the pH is less than 7, the composite material (CS and CPG) will be in the protonated state, facilitating effective adsorption due to the electrostatic attraction between the adsorbate molecule and the adsorbent.

Unfortunately, the adsorptive process for the removal of Cr(VI) could not be carried out nor compared with the chitosan material due to the solubility of CS at pH 3 [5]. This limitation prevented conducting the adsorption experiments under those specific conditions.

3.6.1. Effect of initial metal ion concentration

The experiment involved varying the solution concentration from 20 to 100 mg/l to assess the impact of different metal ion concentrations, specifically Cu(II) and Cr(VI). The analysis was performed at pH 3 for Cr(VI) and pH 7 for Cu(II) while keeping the other variables constant, as illustrated in Figure 7. Initially, as the metal ion concentration increased, the adsorption process on the CPG material intensified, resulting in lower q_e values. This indicated that

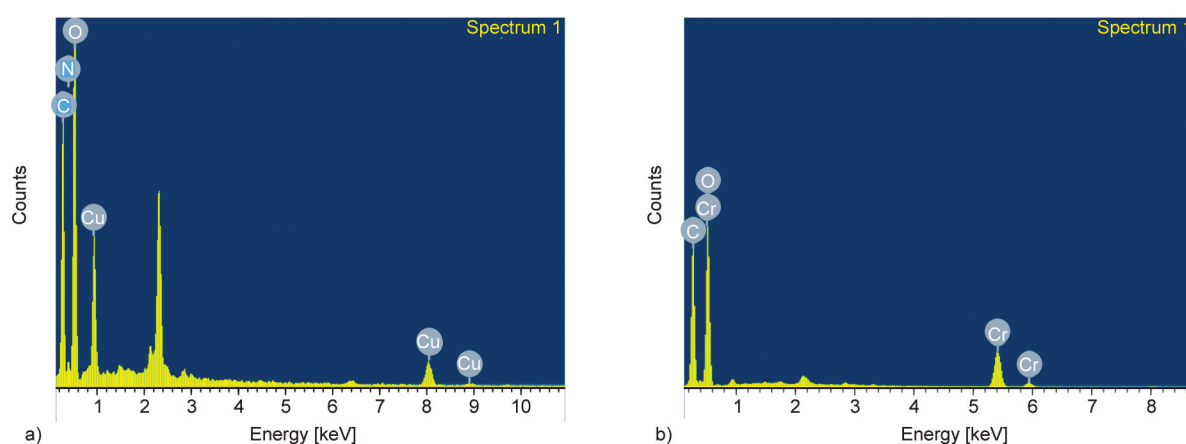


Figure 6. Energy dispersive X-ray spectra of a) Cu(II) and b) Cr(VI) adsorbed on CPG.

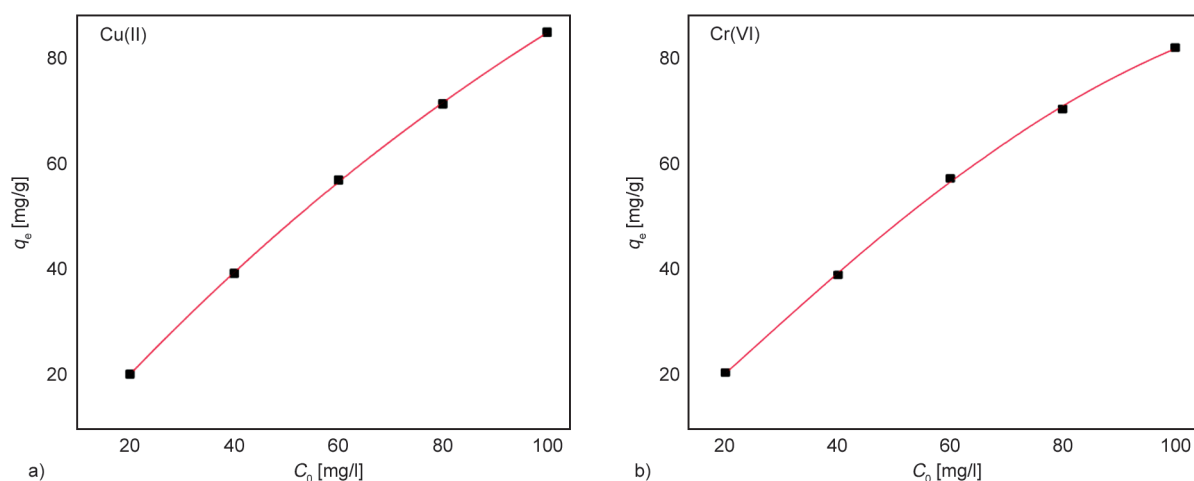


Figure 7. Effect of initial metal ion concentration on the adsorption of a) Cu (II) and b) Cr (VI) on CPG.

the adsorption sites on the CPG were not yet fully saturated with metal ions. However, as the metal ion concentration continued to rise, the graph demonstrated a linear relationship, suggesting that the active sites on the CPG material were now fully saturated with metal ions. The results indicate that the removal process is more efficient when starting with a higher concentration of metal ions. This is because, at a higher concentration, the ions are more readily transferred from the solution to the adsorbent material, maximizing the adsorption capacity [31].

3.6.2. Adsorption kinetic studies

Figure 8 illustrates the variation in the adsorption capacity of metal ions by CPG over time, providing insights into the adsorption mechanism. The graph demonstrates that the adsorption process was rapid initially, attributed to the availability of numerous larger sites for adsorption. As a result, a significant amount of metal ions could quickly be adsorbed onto the CPG material.

However, as time progressed, the adsorption rate gradually decreased. After a certain time interval, the adsorption process reaches a point of saturation due to the exhaustion of available active sites and vacant spaces on the material's surface. At this stage, the adsorption process ceased since no further adsorption sites were available for metal ions to bind, indicating the saturation level was attained. To understand the actual characteristic behaviour of the adsorption process, two well-known kinetic models were employed. These models were used to analyze and interpret the adsorption data, providing valuable insights into the overall adsorption kinetics and the

rate-controlling steps during the process. They were Lagergren's pseudo-first-order model [32] and the Ho's pseudo-second-order model [33].

The Lagergren pseudo-first-order model was employed to analyze the rate of change in the uptake of the adsorbate species with respect to time. Equation (3) represents this model:

$$\frac{dq_t}{dt} = k_1 (q_e - q_t) \quad (3)$$

Integrating the above Equation (3) from $t = 0$ and $q_t = 0$ gives (Equation (4)):

$$\log(q_e - q_t) = \log q_e - \frac{k_1 t}{2.303} \quad (4)$$

where q_e and q_t denote the quantity of adsorbate adsorbed per unit of adsorbent at equilibrium and at various time intervals, respectively. The pseudo-first-order rate constant (k_1) is [min^{-1}], and the adsorption process takes time (t).

Time (t) vs. $\log(q_e - q_t)$ is plotted as a straight line (in Figure 8 not shown), which suggests that the data did not fit well with the corresponding Equation (4) and did not follow the pseudo-first-order kinetics. The coefficient of determination (R^2) values were found to be closer to 1, indicating the best fit for the relevant equation for the pseudo-second-order kinetic model. The surface adsorption process, which is chemical adsorption and where contact occurs as a result of the creation of a chemical bond between the adsorbate molecule and the adsorbent, is the rate-limiting phase in the pseudo-second-order Equation (5):

$$\frac{dq_t}{dt} = k_2 (q_e - q_t)^2 \quad (5)$$

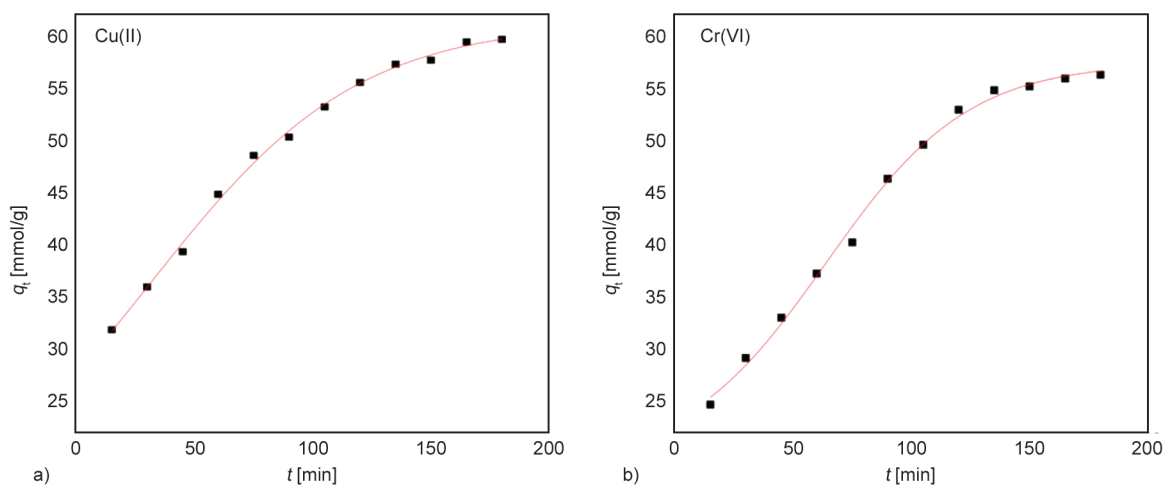


Figure 8. Binding of a) Cu(II) and b) Cr(VI) ions on CPG.

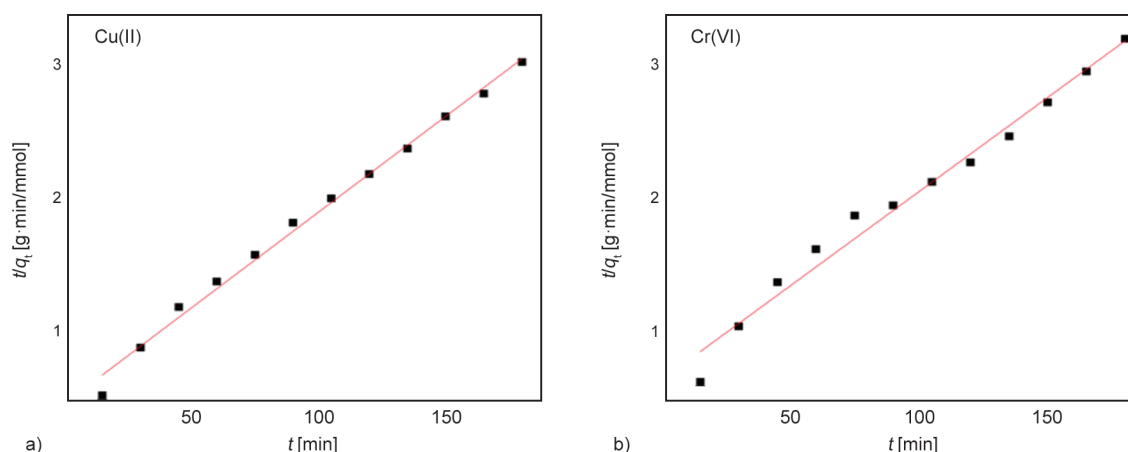


Figure 9. Pseudo Second order kinetics of a) Cu(II) and b) Cr(VI) on CPG.

The integrated form of Equation (5) when $t = 0$ and $q_t = 0$ is Equation (6):

$$\frac{t}{q_t} = \frac{1}{k_2 q_e^2} + \frac{t}{q_e} \quad (6)$$

where k_2 is the second-order rate constant [g/(mg·min)].

Figure 9 illustrates the plot showing the adsorbed ions on the CPG material based on Equation (6), while Table 1 presents the experimental ($q_{e, \text{exp}}$) and theoretical ($q_{e, \text{cal}}$) adsorbate adsorbed per unit of adsorbent at equilibrium and corresponding rate constants. The computed R^2 values in Table 2 demonstrate that

Table 1. Kinetic parameters for the adsorption of Cu(II) and Cr(VI) on CPG.

Metal	Pseudo second order				R^2
	C_0 [mg/l]	$q_{e, \text{exp}}$ [mg/g]	$q_{e, \text{cal}}$ [mg/g]	k_2 [g/(mg·min)]	
Cu(II)	80	71.42	59.62	0.00048	0.993
Cr(VI)	80	71.42	56.37	0.00031	0.981

the pseudo-second-order model exhibited the most accurate linear fit. Furthermore, for both metal ions examined in the study, the estimated q_e values closely matched the observed values, indicating the thorough interaction with the adsorbate and the vacant sites.

3.6.3. Adsorption isotherms

The adsorption experiment was conducted at different concentrations to ascertain the material’s maximum adsorption capability. The rate of adsorption increases as the initial concentration of metal ions increases. The Cu(II) and Cr(VI) ion adsorption isotherms are shown in Figure 10. To analyse the behavior of metal ions on the adsorption surface and to know their interaction and isotherm characteristics, several isotherm models have been utilized, in particular models by Langmuir [34] and Freundlich [35]. The Langmuir adsorption isotherm model accurately describes heterogeneous catalysis and predicts the creation of a monolayer on the adsorption

Table 2. Isotherm parameters for the adsorption of Cu(II) and Cr(VI) on CS and CPG.

(I) CS								
Adsorbate	Langmuir model					Freundlich model		
	C_0 [mg/l]	q_{max} [mg/g]	R_L	K_L [l/mg]	R^2	K_F [l/mg]	n	R^2
Cu(II)	20–100	9.70	2.06	0.01	0.998	1.76	4.065	0.954
(II) CPG								
Adsorbate	Langmuir model					Freundlich model		
	C_0 [mg/l]	q_{max} [mg/g]	R_L	K_L [l/mg]	R^2	K_F [l/mg]	n	R^2
Cu(II)	20–100	166.660	1	0.000036	0.998	30.130	0.676	0.988
Cr(VI)	20–100	142.857	1	0.000144	0.991	4.300	1.570	0.974

surface. According to the Langmuir equation, the adsorption date is given by Equation (7):

$$\frac{C_e}{q_e} = \frac{1}{q_m} C_e + \frac{1}{q_m K_L} \quad (7)$$

where the maximum metal ion adsorbed on the adsorbent surface [mg/g] after adsorption at equilibrium is represented by q_e . While C_e [mg/l] is the equilibrium concentration of adsorbate ions in the solution, K_L [l/mg] is the Langmuir constant, and q_m

is the maximum adsorption capacity when the monolayer forms on the adsorbent surface. The Langmuir isotherm's basic parameter can be calculated using an R_L (constant separation factor), which is given in Equation (8):

$$R_L = \frac{1}{1 + K_L C_0} \quad (8)$$

where C_0 [mg/l] corresponds to the initial concentration of the adsorbent. Figure 11 shows the Langmuir

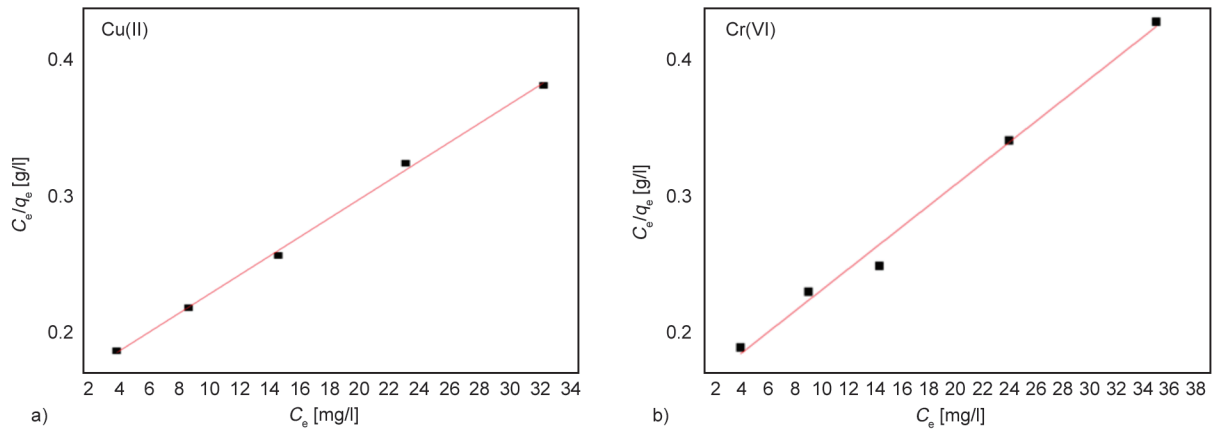


Figure 10. Adsorption isotherms of a) Cu(II) and b) Cr(VI) on CPG.

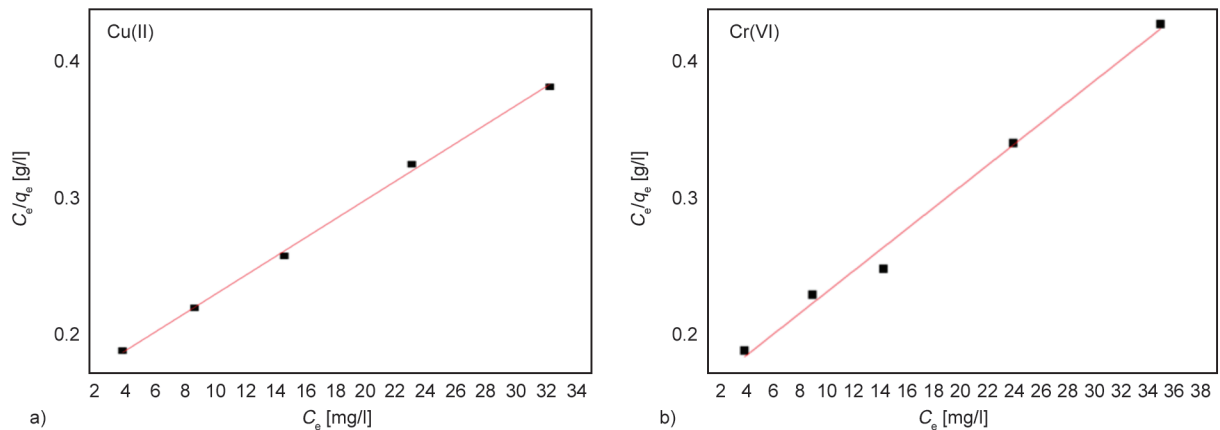


Figure 11. Langmuir isotherm for the adsorption of a) Cu(II) and b) Cr(VI) on CPG.

plots for Cu(II) and Cr(VI) adsorption on CPG. The values obtained for q_m , K_L and R_L are listed in Table 3. The R_L value indicates this model is a favorable adsorption one as the obtained value for the CPG was closer to unity.

According to the Freundlich model, the adsorption process for a given surface area of the adsorbent is given by Equation (9):

$$\log q_e = \log K_F + \frac{1}{n} \log C_e \quad (9)$$

where q_e and C_e have their significance as defined earlier, and K_F is the Freundlich constant [l/mg], which specifies the relative capacity and the adsorption intensity of the adsorbent. The values of K_F and n were obtained by plotting a graph of $\log q_e$ vs. $\log C_e$ (in Figure not shown), and for adsorption parameters of Cr(VI) and Cu(II) obtained from the plot are listed in Table 2.

The isotherm parameters obtained revealed by comparing R^2 values (Table 2) for the fit of the two models that the adsorption data obtained in this case fits best with the Langmuir model, which indicates single-layer binding of Cu(II) and Cr(VI) on the adsorbent surface. Also, based on the q_{\max} values obtained for Cu(II) and Cr(VI), it appears that the adsorption capacity of CS improved significantly after modification.

3.6.4. Comparison studies

The adsorptive behaviour and adsorption capacity depend on the modification of the parent moiety and

also on the presence of functional groups and the hetero atoms which are formed during the modification process. So, the adsorption capacities of various modified adsorbents which have been reported in the literature, are listed in Table 3.

Comparing the results of the present work with the previous literature clearly shows that the synthesized material shows an adsorption capacity of 166.66 and 142.45 mg/g for Cu(II) and Cr(VI), respectively. These values were comparatively higher than many of the previously published data on chitosan adsorbent compounds. The presence of active hetero atoms in the chitosan acts as a good chelating agent. Also, the modification helps for the removal of metal ions and gets the maximum equilibrium adoption capacity.

3.7. Thermodynamic studies

Adsorption and desorption studies were carried out to understand the thermodynamic factors associated with them, with four different temperatures being used to examine the nature of the changes in thermodynamic parameters, such as free energy (ΔG°), enthalpy (ΔH°) and entropy (ΔS°). These are mainly correlated with the adsorption process and were calculated using the standard Equations (10) and (11) presented [47]:

$$\Delta G^\circ = -RT \ln K_c \quad (10)$$

$$\Delta G^\circ = \Delta H^\circ - T\Delta S^\circ \quad (11)$$

where K_c is the equilibrium constant obtained from Equation (12):

Table 3. Adsorption capacity of various chitosan-modified adsorbents for the removal of Cu(II) and Cr(VI).

Adsorbent	q_{\max} [mg/g]		References
	Cr(VI)	Cu(II)	
Chitosan cross-linked with epichlorohydrin		35.5	[35]
Xanthate altered magnetic chitosan		34.5	[36]
Ethylenediamine modified chitosan		38.0	[29]
Chitosan modified with cellulose	13.05	26.50	[37]
Chitosan/cotton fibers		24.78	[38]
Chitosan modified with PVA		47.83	[39]
Chitosan-coated cotton gauze	12.4	14.1	[40]
Calcium(II)-chitosan microspheres		41.5	[41]
Chemically altered chitosan		43.47	[42]
Ethylenediamine cross-linked and magnetic chitosan resin	51.8		[43]
Magnetic chitosan nanoparticles	55.80		[44]
Chitosan-biochar/g-Fe ₂ O ₃ composite (CMB)	167.31		[45]
Heterocyclic alteration of chitosan	85.0	83.75	[46]
Chitosan modified with PVA incorporated with g-C ₃ N ₄	166.66	142.45	Present study

$$K_c = \frac{q_c}{C_c} \quad (12)$$

where q_c , C_c have their meanings as defined earlier. Combining Equations of (10) and (11) gives Equation (13):

$$\ln K_c = \frac{\Delta S^\circ}{R} - \frac{\Delta H^\circ}{RT} \quad (13)$$

where T is the temperature in Kelvin [K], R is the universal gas constant, and ΔH° and ΔS° are the enthalpy and entropy changes during the adsorption process. The resulting plots of the current study are shown in Figure 12 by plotting a graph of $\ln K_{c0}$ vs. $1/T$. The obtained values of change in ΔG° , ΔH° and ΔS° for the binding process of copper Cu(II) and chromium Cr(VI) ions at various temperatures were deduced and are listed in Table 4.

The metal ions Cu(II) and Cr(VI) were adsorbed on the CPG, and the free energy change (G°) during this process was discovered to be negative, suggesting that the adsorption process was spontaneous. In general,

Table 4. Thermo-dynamic parameters for adsorption on CPG.

Adsorbate	T [K]	$\ln K_c$	ΔG° [kJ/mol]	ΔH° [kJ/mol]	ΔS° [J/(mol·K)]
Cu(II)	303	1.28	-3.22	8.77	39.3
	318	1.31	-3.42		
	323	1.38	-3.66		
	328	1.51	-4.06		
Cr(VI)	303	0.89	-2.22	10.04	40.37
	318	0.95	-2.49		
	323	1.04	-2.77		
	328	1.14	-3.06		

the free energy change for physical adsorption falls between -20 and 0 kJ/mol and between -80 and -400 kJ/mol for chemisorption. Obtained ΔG° values demonstrated that the adsorption was intended to proceed in a manner similar to physical adsorption and suggested a favourable adsorption process. A positive value for H° was discovered, indicating an endothermic nature. Additionally, it was discovered that the entropy change value was positive, pointing to a rise in the system's disorder.

3.8. Desorption

In order to assess the stability and reusability of the synthesized materials, experiments were conducted to investigate the repeated adsorption and desorption processes. The regeneration studies involved using experimental solutions with different pH values: a pH of 1.2 for desorbing Cu(II) ions and 0.5 N NaOH (pH 14) for desorbing Cr(VI) ions (Figure 13).

At pH 1.2, 82% of the copper ions were successfully desorbed from the adsorbent surface. This desorption occurred due to the protonation of acid sites on the adsorbent, which resulted in a decreased affinity of the metal ions. The reduced affinity caused the copper ions to be stripped from the adsorbent surface and enter the desorption solution. Consequently, the adsorbent was successfully regenerated and could be reused.

Similarly, at 0.5 N NaOH (pH 14), 85% of the chromium ions were desorbed from the adsorbent material. The desorption process for chromium ions occurred because of the reduced affinity of these metal ions, leading to their stripping from the adsorbent surface and subsequent release into the desorption

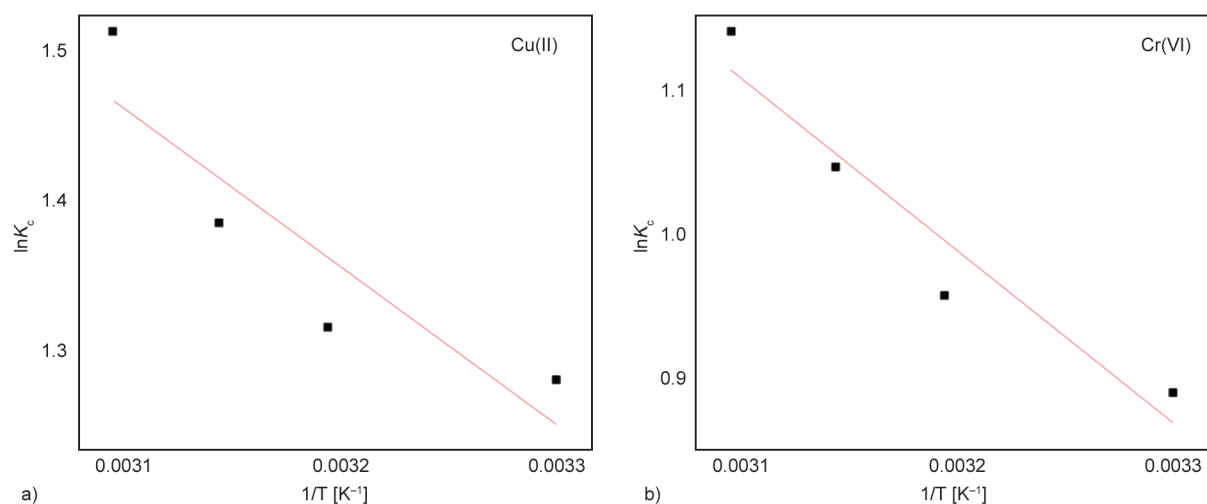


Figure 12. Thermodynamic plots for the uptake of a) Cu(II) and b) Cr(VI) ions by CPG.

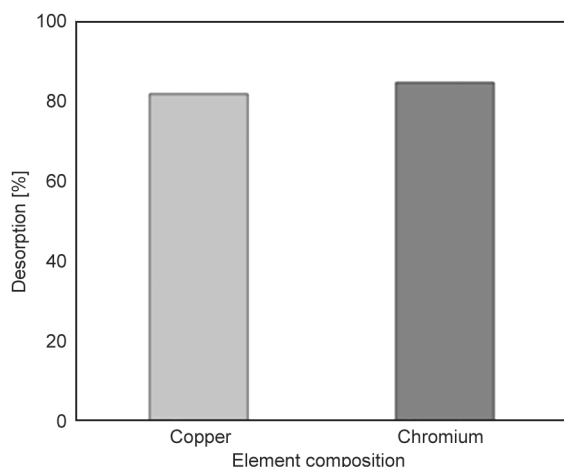


Figure 13. Desorption of Cu(II) and Cr(VI) ions.

solution. As a result, the adsorbent was effectively renewed and could be utilized again for further adsorption cycles.

The high percentages of desorption and successful regeneration indicate that the produced materials are stable and can be repeatedly used for adsorption-desorption cycles without significant loss of adsorption capacity. This reusability feature is crucial for practical applications of the adsorbents in various environmental and industrial settings.

4. Conclusions

In the present study, a novel material known as CPG was successfully synthesized. The formation of a functional nanocomposite material was confirmed through various analyses, including FTIR, TGA, and XRD. The adsorption studies conducted with Cu(II) and Cr(VI) demonstrated that these metal ions effectively bind to the outer surface of the CPG material. The adsorption capacity of CPG was found to be 166.66 mg/g for Cu(II) and 142.85 mg/g for Cr(VI), and the adsorption process followed the Langmuir adsorption isotherm, indicating monolayer adsorption behaviour. Furthermore, the adsorption phenomenon was found to be endothermic, indicating that it required an input of energy to occur. The adsorption process was also spontaneous, meaning it occurred without the need for external intervention. Additionally, the adsorption process was accompanied by a significant increase in entropy, indicating increased disorder in the system. The desorption studies revealed excellent desorbing performance, with approximately 80% recovery of the adsorbed ions. This suggests that adsorbate molecules can be effectively recovered from the CPG material, making it highly

reusable as an adsorbent for repeated adsorption-desorption cycles. Overall, the successful synthesis of CPG and its remarkable adsorption properties, along with the possibility of efficient desorption and reusability, make it a promising nanocomposite adsorbent material for various environmental and industrial applications.

References

- [1] Chen C., Wang X.: Adsorption of Ni(II) from aqueous solution using oxidised multiwall carbon nanotubes. *Industrial and Engineering Chemistry Research*, **45**, 9144–9149 (2006).
<https://doi.org/10.1021/ie060791z>
- [2] Miller J. R., Lechler P. J., Hudson-Edwards K. A., Macklin M. G.: Lead isotopic fingerprinting of heavy metal contamination, Rio Pilcomayo basin, Bolivia. *Geochemistry: Exploration, Environment, Analysis*, **2**, 225 (2002).
<https://doi.org/10.1144/1467-787302-026>
- [3] Gottesfeld P., Cherry C. R.: Lead emissions from solar photovoltaic energy systems in China and India. *Energy Policy*, **39**, 4939 (2011).
<https://doi.org/10.1016/j.enpol.2011.06.021>
- [4] Zhang B., Hu R., Sun D., Wu T., Li Y.: Fabrication of chitosan/magnetite-graphene oxide composites as a novel bioadsorbent for adsorption and detoxification of Cr(VI) from aqueous solution. *Scientific Reports*, **8**, 15397 (2018).
<https://doi.org/10.1038/s41598-018-33925-7>
- [5] Anush S. M., Chandan H. R., Vishalakshi B., Asma, Manju N., Vishalakshi B.: Graphene oxide functionalized chitosan-magnetite nanocomposite for removal of Cu(II) and Cr(VI) from waste water. *International Journal of Biological Macromolecule*, **126**, 4391–4402 (2020).
<https://doi.org/10.1016/j.ijbiomac.2020.09.059>
- [6] Huang B., Liu Y., Li B., Zeng G., Hu X., Zheng B., Li T., Jiang L., Tan X., Zhou L.: Synthesis of graphene oxide decorated with core@double-shell nanoparticles and application for Cr(VI) removal. *RSC Advances*, **5**, 106339–106349 (2015).
<https://doi.org/10.1039/C5RA22862J>
- [7] Schroeder H. A., Tipton I. H.: The human body burden of lead. *Archives of Environmental Health*, **17**, 965 (1968).
<https://doi.org/10.1080/00039896.1968.10665354>
- [8] Wei Y., Zhang Y., Gao X., Yuan Y., Su B., Gao C.: Declining flux and narrowing nanochannels under wrinkles of compacted graphene oxide nanofiltration membranes. *Carbon*, **2016**, 568–575 (2016).
<https://doi.org/10.1016/j.carbon.2016.07.056>
- [9] Fu F., Wang Q.: Removal of heavy metal ions from wastewaters: A review. *Journal of Environmental Management*, **92**, 407 (2011).
<https://doi.org/10.1016/j.jenvman.2010.11.011>

- [10] Cheng Z., Wu Y., Wang N., Yang W., Xu T.: Bromomethylated poly(2,6-dimethyl-1,4-phenylene oxide) (BPPO)-based amphoteric hollow-fiber membranes: Preparation and lysozyme adsorption. *Industrial and Engineering Chemistry Research*, **49**, 3079 (2010).
<https://doi.org/10.1021/ie100348e>
- [11] Ning R. Y.: Arsenic removal by reverse osmosis. *Desalination*, **143**, 237–241 (2002).
[https://doi.org/10.1016/S0011-9164\(02\)00262-X](https://doi.org/10.1016/S0011-9164(02)00262-X)
- [12] Zhao G., Li J., Ren X., Chen C., Wang X.: Few-layered graphene oxide nanosheets as superior sorbents for heavy metal ion pollution management. *Environmental Science and Technology*, **45**, 10454–10462 (2011).
<https://doi.org/10.1021/es203439v>
- [13] Baraka A., Hall P. J., Heslop M. J.: Preparation and characterization of melamine–formaldehyde–DTPA chelating resin and its use as an adsorbent for heavy metals removal from wastewater. *Reactive and Functional Polymers*, **67**, 585–600 (2007).
<https://doi.org/10.1016/j.reactfuncpolym.2007.01.015>
- [14] Dinu M. V., Dragan E. S.: Heavy metals adsorption on some iminodiacetate chelating resins as a function of the adsorption parameters. *Reactive and Functional Polymers*, **68**, 1346–1354 (2008).
<https://doi.org/10.1016/j.reactfuncpolym.2008.06.011>
- [15] Dinu M. V., Dragan E. S., Trochimczuk A. W.: Sorption of Pb(II), Cd(II) and Zn(II) by iminodiacetate chelating resins in non-competitive and competitive conditions. *Desalination*, **249**, 374–379 (2009).
<https://doi.org/10.1016/j.desal.2009.03.016>
- [16] Liu C., Bai R., Ly Q. S.: Selective removal of copper and lead ions by diethylenetriamine-functionalized adsorbent: Behaviors and mechanisms. *Water Research*, **42**, 1511–1522 (2008).
<https://doi.org/10.1016/j.watres.2007.10.031>
- [17] Mezöhegyi G., van der Zee F. P., Font J., Fortuny A., Fabregat A.: Towards advanced aqueous dye removal processes: A short review on the versatile role of activated carbon. *Journal of Environmental Management*, **102**, 148–164 (2012).
<https://doi.org/10.1016/j.jenvman.2012.02.021>
- [18] Bhatt A. S., Sakaria P. L., Vasudevan M., Pawar R. R., Sudheesh N., Bajaj H. C., Mody H. M.: Adsorption of an anionic dye from aqueous medium by organoclays: Equilibrium modeling, kinetic and thermodynamic exploration. *RSC Advances*, **2**, 8663–8671 (2012).
<https://doi.org/10.1039/C2RA20347B>
- [19] Mishra A. K., Arockiadoss T., Ramaprabhu S.: Study of removal of azo dye by functionalized multi walled carbon nanotubes. *Chemical Engineering Journal*, **162**, 1026–1034 (2010).
<https://doi.org/10.1016/j.cej.2010.07.014>
- [20] Shukla N. B., Rattan S., Madras G.: Swelling and dye-adsorption characteristics of an amphoteric superabsorbent polymer. *Industrial and Engineering Chemistry Research*, **51**, 14941–14948 (2012).
<https://doi.org/10.1021/ie301839z>
- [21] Yavuz E., Bayramoğlu G., Arica M. Y., Senkal B. F.: Preparation of poly(acrylic acid) containing core-shell type resin for removal of basic dyes. *Journal of Chemical Technology and Biotechnology*, **86**, 699–705 (2011).
<https://doi.org/10.1002/jctb.2571>
- [22] Li R., Zhang Y., Deng H., Zhang Z., Wang J. J., Shaheend S. M., Xiao R., Rinklebe J., Xi B., He X., Du J.: Removing tetracycline and Hg(II) with ball-milled magnetic nanobiochar and its potential on polluted irrigation water reclamation. *Journal of Hazardous Materials*, **384**, 121095 (2020).
<https://doi.org/10.1016/j.jhazmat.2019.121095>
- [23] Liu G., Jin W., Xu N.: Two-dimensional-material membranes: A new family of high-performance separation membranes. *Angewandte Chemie, International Edition*, **55**, 13384–13397 (2016).
<https://doi.org/10.1002/anie.201600438>
- [24] Meng N., Priestley R. C. V., Zhang Y., Wang H., Zhang X.: The effect of reduction degree of GO nanosheets on microstructure and performance of PVDF/GO hybrid membranes. *Journal of Membrane Science*, **501**, 169–178 (2016).
<https://doi.org/10.1016/j.memsci.2015.12.004>
- [25] Yan H., Yang H., Li A., Cheng R.: pH-tunable surface charge of chitosan/graphene oxide composite adsorbent for efficient removal of multiple pollutants from water. *Chemical Engineering Journal*, **284**, 1397–1405 (2016).
<https://doi.org/10.1016/j.cej.2015.06.030>
- [26] Dutta P. K., Dutta J., Chattopadhyaya M. C., Tripathi V. S.: Chitin and chitosan: Novel biomaterials waiting for future developments. *Journal of Polymer Materials*, **21**, 321–333 (2004).
- [27] Anush S. M., Vishalakshi B.: Modified chitosan gel incorporated with magnetic nanoparticle for removal of Cu(II) and Cr(VI) from aqueous solution. *International Journal of Biological Macromolecules*, **133**, 1051–1062 (2009).
<https://doi.org/10.1016/j.ijbiomac.2019.04.179>
- [28] Shen C., Chen C., Wen T., Zhao Z., Wang X., Xu A.: Superior adsorption capacity of g-C₃N₄ for heavy metal ions from aqueous solutions. *Journal of Colloid and Interface Science*, **456**, 7–14 (2015).
<https://doi.org/10.1016/j.jcis.2015.06.004>
- [29] Vishnu G., Naik H. S. B., Viswanath R., Kirthan B. R., Nayak P. H. A., Bajiri M. A.: Combustion-assisted green-synthesized magnesium-doped cadmium ferrite nanoparticles for multifunctional applications. *New Journal of Chemistry*, **46**, 1943–1959 (2022).
<https://doi.org/10.1039/D1NJ05156C>
- [30] Chethan P. D., Vishalakshi B.: Synthesis of ethylenediamine modified chitosan microspheres for removal of divalent and hexavalent ions. *International Journal of Biological Macromolecules*, **75**, 179–185 (2015).
<https://doi.org/10.1016/j.ijbiomac.2015.01.032>

- [31] Dönmez Ç. G., Aksu Z., Öztürk A., Kutsal T.: A comparative study on heavy metal biosorption characteristics of some algae. *Process Biochemistry*, **34**, 885–892 (1999).
[https://doi.org/10.1016/S0032-9592\(99\)00005-9](https://doi.org/10.1016/S0032-9592(99)00005-9)
- [32] Yao Z-Y., Qi J-H., Wang L-H.: Equilibrium, kinetic and thermodynamic studies on the biosorption of Cu(II) onto chestnut shell. *Journal of Hazardous Materials*, **174**, 137–143 (2010).
<https://doi.org/10.1016/j.jhazmat.2009.09.027>
- [33] Ho Y. S., McKay G.: Pseudo-second order model for sorption processes. *Process Biochemistry*, **34**, 451–465 (1999).
[https://doi.org/10.1016/S0032-9592\(98\)00112-5](https://doi.org/10.1016/S0032-9592(98)00112-5)
- [34] Langmuir I.: The adsorption of gases on plane surfaces of glass, mica and platinum. *Journal of the American Chemical Society*, **40**, 1361–1403 (1918).
<https://doi.org/10.1021/ja02242a004>
- [35] Freundlich H.: Über die Adsorption in Lösungen. *Zeitschrift für Physikalische Chemie*, **57**, 385–470 (1906).
<https://doi.org/10.1515/zpch-1907-5723>
- [36] Chen A-H., Liu S-C., Chen C-Y.: Comparative adsorption of Cu(II), Zn(II), and Pb(II) ions in aqueous solution on the crosslinked chitosan with epichlorohydrin. *Journal of Hazardous Materials*, **154**, 184–191 (2008).
<https://doi.org/10.1016/j.jhazmat.2007.10.009>
- [37] Zhu Y., Hu Y., Wang J.: Competitive adsorption of Pb(II), Cu(II) and Zn(II) onto xanthate-modified magnetic chitosan. *Journal of Hazardous Materials*, **221–222**, 155–161 (2012).
<https://doi.org/10.1016/j.jhazmat.2012.04.026>
- [38] Wan Ngah W. S., Teong L. C., Hanafiah M. A. K. M.: Adsorption of dyes and heavy metal ions by chitosan composites: A review. *Carbohydrate Polymers*, **83**, 1446–1456 (2011).
<https://doi.org/10.1016/j.carbpol.2010.11.004>
- [39] Ngah W. S. W., Kamari A., Koay Y. J.: Equilibrium and kinetics studies of adsorption of copper (II) on chitosan and chitosan/PVA beads. *International Journal of Biological Macromolecules*, **34**, 155–161 (2004).
<https://doi.org/10.1016/j.ijbiomac.2004.03.001>
- [40] Ferrero F., Tonetti C., Periolatto M.: Adsorption of chromate and cupric ions onto chitosan-coated cotton gauze. *Carbohydrate Polymers*, **110**, 367–373 (2014).
<https://doi.org/10.1016/j.carbpol.2014.04.016>
- [41] He J., Lu Y., Luo G.: Ca(II) imprinted chitosan microspheres: An effective and green adsorbent for the removal of Cu(II), Cd(II) and Pb(II) from aqueous solutions. *Chemical Engineering Journal*, **244**, 202–208 (2014).
<https://doi.org/10.1016/j.cej.2014.01.096>
- [42] Kannamba B., Reddy K. L., AppaRao B. V.: Removal of Cu(II) from aqueous solutions using chemically modified chitosan. *Journal of Hazardous Materials*, **175**, 939–948 (2009).
<https://doi.org/10.1016/j.jhazmat.2009.10.098>
- [43] Hu X-J., Wang J-S., Liu Y-G., Li X., Zeng G-M., Bao Z-L., Zeng X-X., Chen A-W., Long F.: Adsorption of chromium (VI) by ethylenediamine-modified cross-linked magnetic chitosan resin: Isotherms, kinetics and thermodynamics. *Journal of Hazardous Materials*, **185**, 306–314 (2011).
<https://doi.org/10.1016/j.jhazmat.2010.09.034>
- [44] Thinh N. N., Hanh P. T. B., Ha L. T. T., Anh L. N., Hoang T. V., Hoang V. D., Dang L. H., Khoi N. V., Lam T. D.: Magnetic chitosan nanoparticles for removal of Cr(VI) from aqueous solution. *Materials Science and Engineering: C*, **33**, 1214–1218 (2013).
<https://doi.org/10.1016/j.msec.2012.12.013>
- [45] Ming M Z., Yun G L., Ting T L., Wei H X., Bo H Z., Xiao F T., Hui W., Yi M G., Fang Y G., Shu F W.: Chitosan modification of magnetic biochar produced from *Eichhornia crassipes* for enhanced sorption of Cr(VI) from aqueous solution. *RSC Advances*, **5**, 46955–46964, (2015).
<https://doi.org/10.1039/C5RA02388B>
- [46] Anush S. M., Vishalakshi B., Chandan H. R., Geetha B. R.: Heterocyclic modification of chitosan for the adsorption of Cu(II) and Cr(VI) ions. *Separation Science and Technology*, **53**, 1979–1990 (2018).
<https://doi.org/10.1080/01496395.2018.1442859>
- [47] Kara A., Demirbel E., Tekin N., Osman B., Beşirli N.: Magnetic vinylphenyl boronic acid microparticles for Cr(VI) adsorption: Kinetic, isotherm and thermodynamic studies. *Journal of Hazardous Materials*, **286**, 612–623 (2015).
<https://doi.org/10.1016/j.jhazmat.2014.12.011>